N-terminal tags impair the ability of Lamin A to provide structural support to the nucleus

Jacob Odell[1,2], Jan Lammerding[1,3,*]

[1]Weill Institute for Cell and Molecular Biology, Cornell University, Ithaca, NY 14853; [2]Graduate Field of Biochemistry, Molecular and Cell Biology, Cornell University, Ithaca, NY 14853; [3]Meinig School of Biomedical Engineering, Cornell University, Ithaca, NY 14853

[*] Contact information: jan.lammerding@cornell.edu

Abstract

Lamins are intermediate filament proteins that contribute to numerous cellular functions, including nuclear morphology and mechanical stability. The N-terminal head domain of lamin is critical for higher order filament assembly and function, yet the effects of commonly used N-terminal tags on lamin function remain largely unexplored. Here, we systematically studied the effect of two differently sized tags on Lamin A (LaA) function in a mammalian cell model engineered to allow for precise control of expression of tagged lamin proteins. Untagged, FLAG-tagged, and GFP-tagged LaA completely rescued nuclear shape defects when expressed at similar levels in lamin A/C-deficient (*Lmna*$^{-/-}$) MEFs, and all LaA constructs prevented increased nuclear envelope ruptures in these cells. The N-terminal tags, however, altered the nuclear localization of LaA and impaired the ability of LaA to restore nuclear deformability and to recruit Emerin to the nuclear membrane in *Lmna*$^{-/-}$ MEFs. Our finding that tags impede some LaA functions but not others may explain the partial loss of function phenotypes when tagged lamins are expressed in model organisms and should caution researchers using tagged lamins to study the nucleus.

Keywords: nucleus, lamins, fluorescent tags, emerin, GFP, mechanobiology

Introduction

Lamins are nuclear intermediate filament proteins that form a dense protein meshwork underlying the inner nuclear membrane (Aebi et al., 1986; Buxboim et al., 2023; Shimi et al., 2015). Lamins have many important functions in metazoan cells, where they provide structural support to the nucleus and regulate nuclear morphology, contribute to nuclear mechanics, and influence gene expression (de Leeuw et al., 2018; Kalukula et al., 2022; Vahabikashi et al., 2022). Vertebrate lamins are grouped into A-type and B-type lamins, which differ in their expression patterns, interaction partners, and effect on nuclear mechanical properties (Buxboim et al., 2023; Odell and Lammerding, 2023). Research on lamins frequently involves the addition of a tag, i.e., the fusion of a genetically encoded fluorophore or epitope tag to the lamin protein, to allow for detection in live cells and other assays, yet growing evidence suggests that the addition of tags may alter the behavior of the protein of interest. Like other proteins, lamins are sensitive to where the tag is placed within the protein sequence (Herrmann et al., 2002). C-terminal tags lead to obvious loss of function phenotypes, as the tag disrupts the lamin C-terminal CaaX motif important for proper post-translational processing and localization of lamins (Kreplak et al., 2008). Furthermore, in the case of LaA, C-terminal tags are not suitable as the end of prelamin A is cleaved during processing into mature LaA (Sinensky et al., 1994). Consequently, the vast majority of studies use N-terminal tags to label LaA. For example, N-terminally tagged lamins have been used to visualize the localization and dynamics of lamins in live cells throughout the cell cycle (Broers et al., 1999), study interactors of lamins (Roux et al., 2012), investigate autophagy (Dou et al., 2015), and to serve as a marker of the nucleus in live cells and organisms (Morin et al., 2001; Rizzo et al., 2009). Furthermore, fluorescently tagged lamins have been used to visualize lamin networks and to study the effect of specific lamin mutations on network assembly and dynamics (Kono et al., 2022; Shimi et al., 2015).

Although key findings from these studies have been confirmed by immunostaining for endogenous, untagged lamins, various studies using tagged lamin in model organisms suggest that the presence of a tag can be detrimental for proper lamin assembly and function. In the nematode *C. elegans*, endogenous tagging of its lone lamin with GFP at the N-terminus causes mild or moderate fitness defects (Bone et al., 2016) and abnormal lamina assembly and stability (Velez-Aguilera et al., 2020). A recent report where *C. elegans* lamin was tagged at the N-terminus with a small split-GFP, i.e., the 11th beta strand of GFP, showed no detrimental effect on organismal viability, yet the animals expressing the tagged lamin still had mild swimming defects, indicating a partial loss of function (Gregory et al., 2023). GFP-tagged lamins have also been associated with impaired function in *Drosophila*, as endogenously tagged GFP-LamC marks the nuclear envelope as expected, but leads to bright nuclear granules (Morin et al., 2001; Schulze et al., 2005) and abnormal chromatin patterns (Gurudatta et al., 2010), suggesting that the chimeric protein has compromised function. No other fly lines with endogenously tagged lamins have been reported, and no commercially available mice with endogenously tagged lamin(s) exist, suggesting that tags may be broadly detrimental for organism viability. However, no systematic comparison of differently sized N-terminal tags on mammalian lamins has been performed to date, and many of the early studies using fluorescently tagged mammalian lamins involved overexpression of tagged

lamin in a background of endogenous untagged lamins, which may mask loss-of-function effects of the tag on lamins.

To address these knowledge gaps, we determined the effects of differently sized N-terminal tags on LaA function in a mammalian cell model. Well-defined, inducible expression of untagged and tagged LaA constructs in lamin A/C-deficient (*Lmna*$^{-/-}$) mouse embryo fibroblasts (MEFs) enabled us to test whether the tag compromised specific functions of LaA. Specifically, we examined differences in rescue potential of LaA with a small N-terminal tag (FLAG: 8 amino acids, 1 kDa) or large N-terminal tag (enhanced GFP: 238 amino acids, 27 kDa) compared to untagged LaA and assessed these proteins' ability to rescue nuclear morphology, deformability, rupture, and disturbed localization of lamin-interacting proteins in *Lmna*$^{-/-}$ MEFs. We found that all LaA constructs were capable of completely rescuing nuclear shape defects and reversing nuclear envelope ruptures that arise upon loss of lamin A/C. However, only untagged LaA was able to completely rescue all functional defects, and cells expressing N-terminal tagged LaA exhibited altered nuclear LaA distribution and only limited rescue in nuclear deformability and restoring nuclear envelope localization of Emerin. Our surprising finding that tags impede some lamin functions but not others highlights the importance of the N-terminus in proper LaA function and provides a likely explanation for the partial loss of function phenotypes observed when tagged lamins are used in model organisms.

Results and Discussion

Loss of lamin A/C leads to abnormal nuclear shapes, increased rates of spontaneous nuclear envelope rupture, decreased nuclear stiffness, and displacement of lamin-interacting proteins such as Emerin from the nuclear envelope (Borin et al., 2020; Earle et al., 2020; Lammerding et al., 2006; Sullivan et al., 1999; Wintner et al., 2020; Zwerger et al., 2013). One of the best characterized systems are *Lmna*$^{-/-}$ MEFs (Sullivan et al., 1999), which are ideally suited for morphological and functional studies (Chen et al., 2021, 2018; Coffinier et al., 2010; Lammerding et al., 2006, 2004; Odell et al., 2024; Zwerger et al., 2013). In these cells, nuclear defects can be rescued by re-introduction of human LaA (Lammerding et al., 2006; Odell et al., 2024; Wintner et al., 2020). To systematically assess the effect of different N-terminal tags on the ability of exogenously expressed LaA to rescue nuclear defects in *Lmna*$^{-/-}$ MEFs, we generated expression constructs to allow for the inducible expression of untagged human LaA, FLAG [DYKDDDDK]-LaA, or GFP-LaA under the control of a doxycycline-inducible promoter (Figure 1A). These vectors were then stably introduced into *Lmna*$^{-/-}$ MEFs, and the resulting cell populations were clonally derived to acquire populations of cells with tunable expression levels (Figure 1A-B). This inducible system following clonal derivation has been shown previously to be effective to yield approximately equal levels of protein expression, following titration of doxycycline concentrations (Odell et al., 2024). Precisely controlling the expression levels of the exogenously expressed lamin constructs is crucial for quantitative comparison, since previous studies showed that LaA expression levels directly correlate with nuclear stiffness (Lammerding et al., 2006; Srivastava et al., 2021; Swift et al., 2013) and that severe overexpression of GFP-tagged lamins can cause aggregation and mislocalization (Rizzo et al., 2009). Using the *Lmna*$^{-/-}$ MEFs with inducible LaA expression constructs, we identified individual clones and specific doxycycline concentrations that

yielded similar levels of LaA expression across the differently tagged constructs and that resulted in expression levels comparable to wild-type LaA in *Lmna*$^{+/+}$ MEFs (Figure 1B-D). Due to potential difference in epitope recognition between human and mouse LaA, we cannot exclude the possibility that the levels of the human LaA differ somewhat from the endogenous mouse LaA, but nonetheless our studies confirm that all three exogenous constructs were expressed at similar levels in the *Lmna*$^{-/-}$ MEFs. To ensure that the different clones did not exhibit phenotypic differences at baseline, we included a "no dox" control for each clonal cell line for all functional assays with the *Lmna*$^{-/-}$ MEFs.

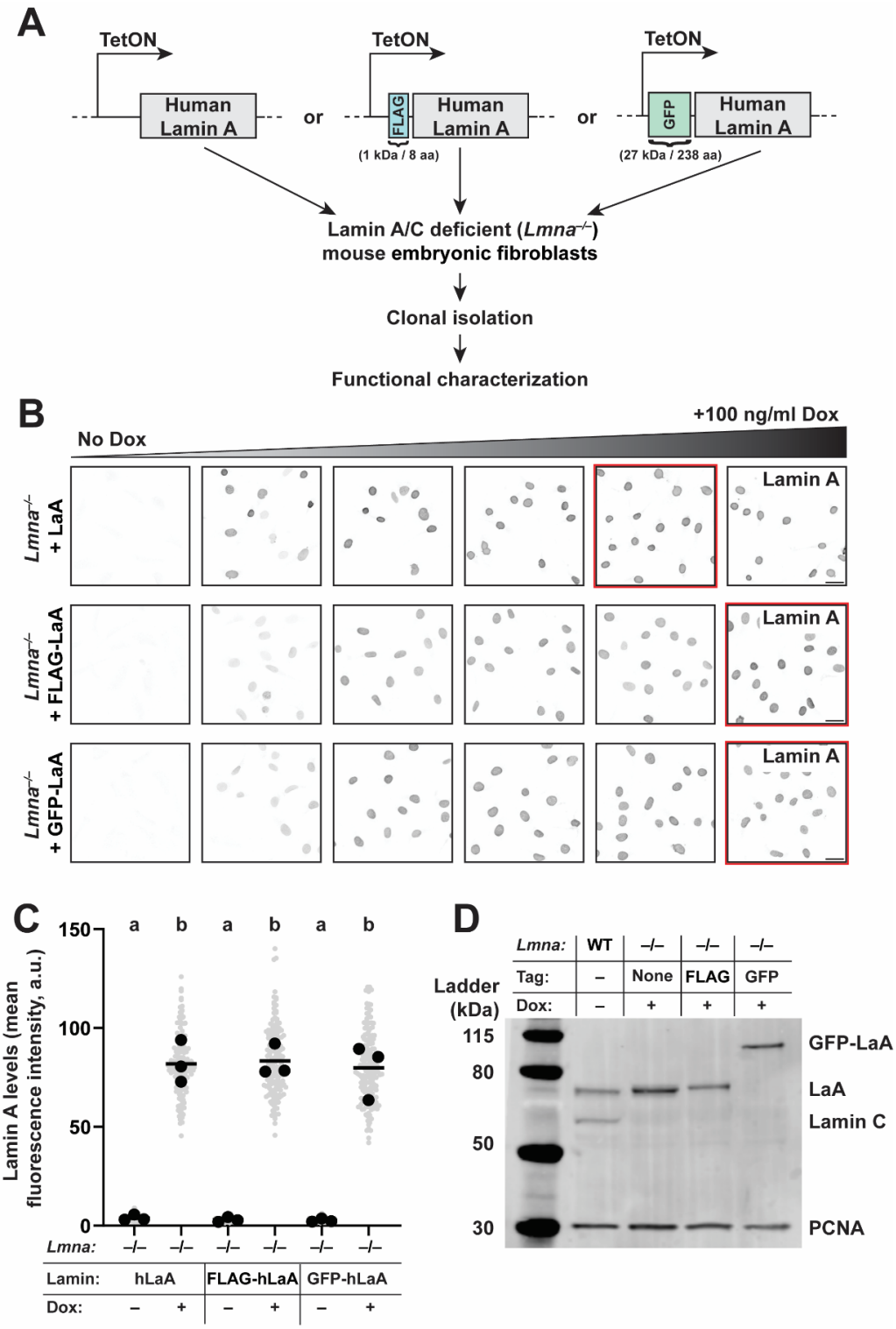

Figure 1: Expressing tagged LaA constructs at defined levels. (**A**) Overview of lamin constructs, exogenous expression system, and experimental pipeline to compare the effect of different N-terminal tags on lamin A (LaA) function. (**B**) Induction of exogenous LaA was induced in clonal *Lmna*$^{-/-}$ MEFs following titration of doxycycline levels from 0, 6.25, 12.5, 25, 50, to 100 ng/ml. Conditions that resulted in similar levels of LaA expression are highlighted by a red bounding box. Scale bar: 50 µm. (**C**) Quantification of LaA levels by immunofluorescence

staining. Cells were treated with the concentrations of doxycycline identified in (**B**). Nuclei were identified based on DAPI staining, and average nuclear LaA intensity is shown based on immunofluorescence staining. (**D**) Immunoblot analysis showing similar levels of LaA expression between the different cell lines/constructs, following treatment with doxycycline levels identified in (**B**). PCNA was used as a loading control. Grey points represent measurements from individual cells, black points represent replicate means, and bars indicate overall means. Letters above each set of points indicate results of One-way ANOVA with Tukey's multiple comparison test, performed on the replicate means. Sets of points with the same letter above them are not statistically significantly different, whereas different letters indicate $p < 0.05$.

Nuclear morphology and LaA distribution in cells expressing differently tagged LaA constructs

All three LaA constructs localized to the nucleus and were enriched at the nuclear periphery as expected (Figure 2A). We previously showed that loss of lamin A/C results in abnormally shaped nuclei with decreased nuclear circularity (Lammerding et al., 2006; Odell et al., 2024; Zwerger et al., 2013). Expression of all three LaA constructs increased nuclear circularity in *Lmna*$^{-/-}$ MEFs (Figure 2B), indicating function rescue. Notably, we did not detect any difference in the circularity of nuclei prior to inducing LaA expression, and all LaA constructs, regardless of the presence of a tag, showed similar efficacy in restoring nuclear shape to levels of wild-type cells (Figure 2B).

Impaired lamin filament assembly can result in altered intranuclear distribution, such as loss of LaA from the nuclear envelope and an increase in nucleoplasmic LaA (Manju et al., 2006; Wallace et al., 2023; Zwerger et al., 2015, 2013). To assess the effect of the different tags on intranuclear localization of LaA, we measured the intensity profiles of LaA across the nucleus following indirect immunofluorescence staining with a LaA specific antibody that recognizes an epitope present in all three LaA constructs (Figure 2C). The three LaA constructs were enriched at the nuclear periphery to similar extents, but both FLAG-LaA and GFP-LaA had increased nucleoplasmic localization compared to the untagged LaA construct (Figure 2A, C, D). This finding suggests that the addition of a tag to the N-terminus of human LaA may interfere with proper LaA assembly into the nuclear lamina. These results are in agreement with previous studies, which reported defects in the assembly and/or localization when using lamins with an N-terminal GFP-tag (Morin et al., 2001; Velez-Aguilera et al., 2020).

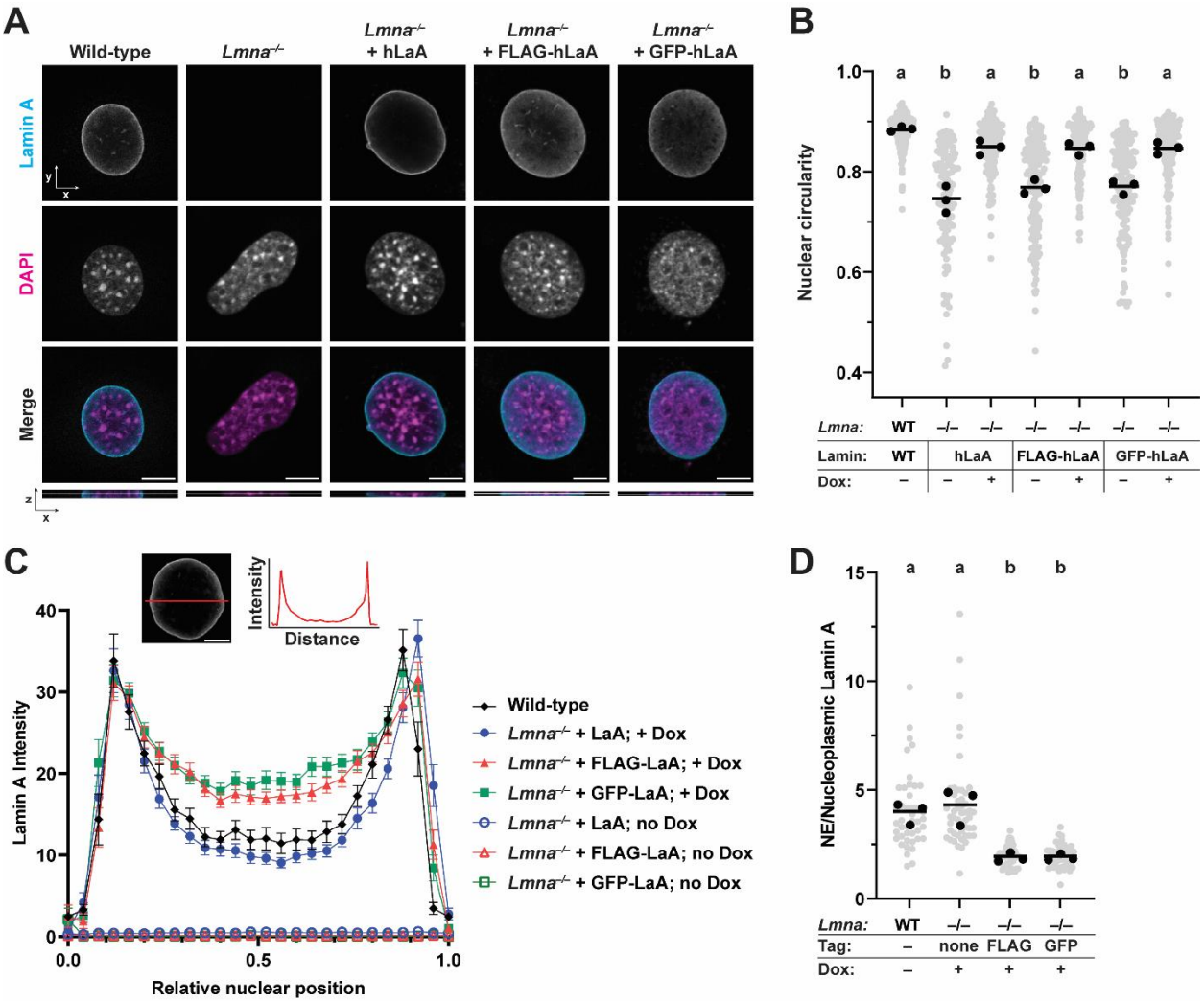

Figure 2: N-terminal tags interfere with proper localization of LaA. (**A**) Representative immunofluorescence images of cells immunofluorescently labeled for LaA. Single confocal z-slices are shown, with the orthoview shown below each set of images. The horizontal white line through each orthoview indicates the plane shown in the main figure. Scale bar: 10 µm. (**B**) Nuclear circularity analysis of cells expressing different LaA constructs, using the doxycycline conditions identified in Figure 1. (**C**) Quantification of LaA intensity profiles along a line through the midplane of the nucleus (see red line in top left inset). All cells were immunofluorescently labeled with a LaA-specific antibody, as in Figure 1. The graph depicts the LaA intensity as a function of relative position within the nucleus along the line spanning the width of the nucleus. The peaks at the edges of the plot reflect the nuclear lamina, and the center of the plot reflects nucleoplasmic signal. Note that in the "no-dox" conditions, the *Lmna*$^{-/-}$ MEFs do not express LaA, and thus no signal is visible in this assay. (**D**) Quantification of LaA fluorescence intensity ratio between the nuclear envelope (NE) and nucleoplasmic LaA signal for the cell lines shown in (**C**). Grey points represent measurements from individual cells, black points represent replicate means, and bars indicate overall means. Letters above each set of points indicate results of One-way ANOVA with Tukey's multiple comparison test, performed on the replicate means. Sets of points with the same letter above them are not significantly different, whereas different letters indicate $p < 0.05$.

N-terminal tags interfere with LaA's ability to rescue nuclear stiffness

Lamins are an important contributor to nuclear deformability, and loss of lamin A/C leads to nuclei with decreased nuclear stiffness (Davidson et al., 2019; Earle et al., 2020; Lammerding et al., 2006; Pajerowski et al., 2007; Wintner et al., 2020). To assess the effect of different tags on LaA's ability to rescue nuclear stiffness in *Lmna*$^{-/-}$ MEFs, we applied a recently developed high-throughput micropipette aspiration assay (Davidson et al., 2019) to these cells, which imposes large deformations on the nucleus (Figure 3A-B). Whereas small nuclear deformations are predominantly resisted by chromatin, large nuclear deformations are primarily resisted by lamins (Stephens et al., 2017), making this assay ideally suited to measure the mechanical function of lamins. At baseline (i.e., without induction of exogenous LaA), all *Lmna*$^{-/-}$ clonal MEF lines had similar levels of nuclear deformability, and all *Lmna*$^{-/-}$ MEF lines were more deformable than wild-type cells (Figure 3A-D). All three LaA constructs were able to rescue nuclear deformability at least partially compared to the non-induced controls (Figure 3A-D). However, only untagged LaA was able to restore nuclear deformability to wild-type levels (Figure 3D). Despite the large difference in size, both the FLAG-tag and the GFP-tag resulted in similar levels of (partial) rescue. These results suggest that the addition of an N-terminal tag, even as small as a FLAG-tag, inhibits the ability of LaA to regulate nuclear stiffness.

In addition to having more deformable nuclei, cells lacking lamin A/C have increased rates of nuclear envelope rupture in both in vivo and in vitro models (Cho et al., 2019; De Vos et al., 2011; Denais et al., 2016; Earle et al., 2020; Raab et al., 2016). We examined the ability of the different LaA constructs to reduce the rate of spontaneous nuclear envelope rupture in *Lmna*$^{-/-}$ MEFs using a fluorescent reporter for nuclear envelope rupture consisting of cyclic GMP-AMP synthase (cGAS) fused with mCherry (Denais et al., 2016; Odell et al., 2024; Raab et al., 2016). cGAS is a cytosolic protein that accumulates at sites where nuclear DNA is exposed to the cytoplasm (Figure 3E). The cGAS-mCherry reporter contains two mutations (E225A/D227A) introduced into the cGAS catalytic domain that prevent interferon production and downstream immune signaling, while still allowing for the protein to bind DNA and localize at nuclear envelope rupture sites (Denais et al., 2016). Consistent with previous studies, we found that *Lmna*$^{-/-}$ MEFs had increased rates of spontaneous nuclear envelope rupture compared to wild-type controls (Figure 3F). Expression of either untagged LaA, FLAG-LaA, or GFP-LaA reduced the nuclear envelope rupture rates in *Lmna*$^{-/-}$ MEFs (Figure 3F). Surprisingly, despite their different effects on nuclear deformability, all LaA constructs were able to restore nuclear envelope rupture rates in *Lmna*$^{-/-}$ MEFs to levels of wild-type MEFs, suggesting that the addition of an N-terminal tag does not interfere with LaA's ability to maintain nuclear membrane integrity.

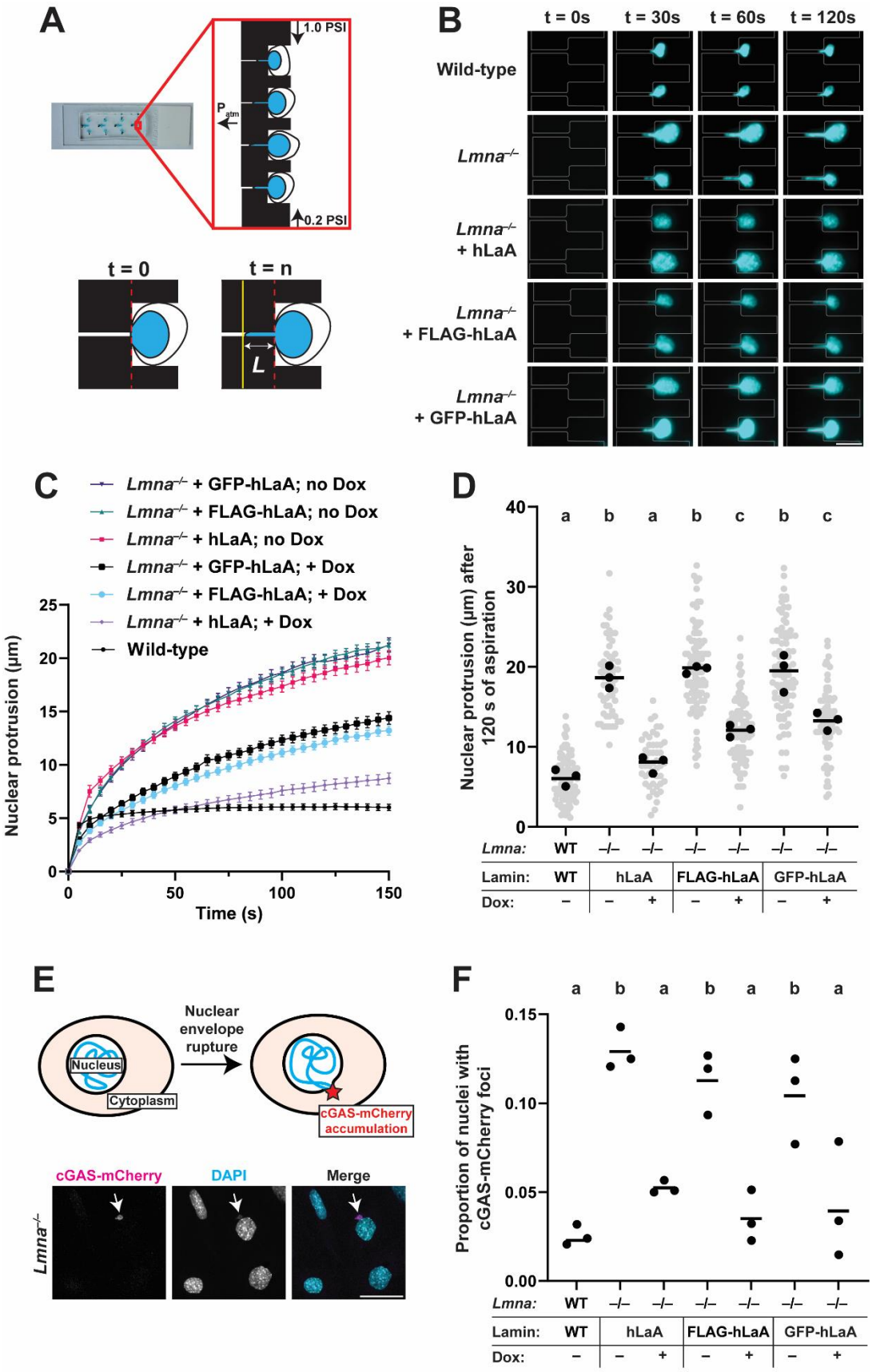
A
1.0 PSI
P_{atm}
0.2 PSI
t = 0
t = n
L
B
t = 0s
t = 30s
t = 60s
t = 120s
Wild-type
Lmna−/−
Lmna−/− + hLaA
Lmna−/− + FLAG-hLaA
Lmna−/− + GFP-hLaA
C
Lmna−/− + GFP-hLaA; no Dox
Lmna−/− + FLAG-hLaA; no Dox
Lmna−/− + hLaA; no Dox
Lmna−/− + GFP-hLaA; + Dox
Lmna−/− + FLAG-hLaA; + Dox
Lmna−/− + hLaA; + Dox
Wild-type
Nuclear protrusion (µm)
Time (s)
D
Nuclear protrusion (µm) after 120 s of aspiration
Lmna:
Lamin:
Dox:
WT
hLaA
FLAG-hLaA
GFP-hLaA
E
Nuclear envelope rupture
Nucleus
Cytoplasm
cGAS-mCherry accumulation
cGAS-mCherry
DAPI
Merge
Lmna−/−
F
Proportion of nuclei with cGAS-mCherry foci

Figure 3: N-terminal tag impairs ability of LaA to rescue nuclear stiffness, but not nuclear envelope rupture. (**A**) Schematic of microfluidic micropipette aspiration assay. Adapted from (Odell et al., 2024). In brief, a cell suspension was perfused into the device under a precisely controlled pressure gradient, and cells were forced to deform through micropipette channels 3 µm × 5 µm in cross-section. The protrusion of the nucleus into the channel over time provides information on the nuclear mechanical properties. (**B**) Time-dependent nuclear protrusion during micropipette aspiration. Nuclei were stained with Hoechst (cyan) and aspirated for the indicated time periods. Grey outlines indicate boundaries of micropipette channels. Nuclei of *Lmna*$^{-/-}$ MEFs deform substantially more than those of wild-type cells, with exogenously expressed LaA reducing nuclear deformation in the *Lmna*$^{-/-}$ MEFs. Scale bar: 20 µm. (**C**) Quantification of nuclear protrusion over time, with t = 0 being the first frame when cells entered the micropipette channel. Plots depict mean nuclear protrusion length from three independent experiments; error bars represent s.e.m.. Statistical analysis for 120 s time point provided in panel D. (**D**) Nuclear protrusion lengths at t = 120 s after the start of aspiration. Grey points represent measurements from individual cells, black points represent means of independent experiments, and bars indicate overall means. Letters above each set of points indicate results of One-way ANOVA with Tukey's multiple comparison test, performed on the replicate means. Sets of points with the same letter above them are not significantly different, whereas different letters indicate $p < 0.05$. (**E**) Schematic overview of cGAS-mCherry reporter function and corresponding representative images if *Lmna*$^{-/-}$ MEFs expressing cGAS-mCherry reporter. Arrowhead indicates site of nuclear rupture, where a cGAS-mCherry puncta overlaps with DNA (DAPI) spilling into the cytoplasm. Scale bar: 50 µm. (**F**) Quantification of nuclear envelope rupture rate, i.e., the fraction of cells experiencing nuclear envelope rupture determined by the presence of mCherry signal adjacent to a DAPI stained nucleus. Individual data points indicate means from independent experiments; bars indicate overall proportions based on three independent experiments. At least 180 nuclei in total were scored for each cell line. Different letters above each set of points indicate $p < 0.05$ based on Fisher's exact test.

N-terminal tags interfere with ability of LaA to localize and interact with Emerin

Emerin is an inner nuclear envelope protein and a known LaA interactor that is retained at the inner nuclear membrane (INM) by lamin A/C (Fernandez et al., 2022; Liddane and Holaska, 2021). In *Lmna*$^{-/-}$ MEFs, Emerin was mislocalized from the nuclear envelope and primarily distributed to the cytoplasm (Figure 4A-B), consistent with previous reports (Guo et al., 2014; Sullivan et al., 1999; Vaughan et al., 2001). Nuclear envelope localization of Emerin can be restored by exogenous expression of LaA in *Lmna*$^{-/-}$ MEFs (Odell et al., 2024; Östlund et al., 2006). Here, we determined the ability of the different LaA constructs to restore proper nuclear envelope localization of Emerin. In the absence of LaA expression ('no dox'), all clonal *Lmna*$^{-/-}$ MEFs had similar levels of Emerin mislocalization (Figure 4B). Upon expression, all three LaA constructs increased the presence of Emerin at the nuclear envelope, but only the untagged LaA and the FLAG-LaA constructs were able to fully restore wild-type levels of Emerin at the nuclear envelope (Figure 4B-C). The incomplete rescue achieved in this assay by the GFP-LaA construct was akin to the partial rescue observed with the GFP-LaA construct in the micropipette assay for mechanical deformability. In contrast, expression of FLAG-LaA completely rescued Emerin localization despite only a partial rescue in the micropipette assay. These results suggest that the presence of the large N-terminal GFP tag may interfere with the proper association of LaA with Emerin, whereas the smaller FLAG tag may not disturb this interaction. To determine if the large N-terminal GFP-tag impaired *in vitro* binding between LaA and Emerin, we performed co-immunoprecipitation analysis using lysates from each of the cell lines expressing different LaA constructs. For these experiments, we induced LaA, FLAG-LaA, or GFP-LaA expression for 24 hours, lysed the cells, and immunoprecipitated LaA as bait using a LaA-specific antibody. Emerin

co-immunoprecipitated with the untagged LaA at much higher levels than with the FLAG-LaA or GFP-LaA constructs (Figure 4D-E). Despite FLAG-LaA being able to fully rescue nuclear Emerin localization in cells, FLAG-LaA had a limiting effect on the interaction of LaA with Emerin measured by co-IP. It is important to note that these orthogonal approaches probe for different abilities of LaA to bind Emerin. In cells, Emerin can interact with fully assembled LaA filaments near the nuclear membranes, whereas in cell lysates, the nuclear envelope is disrupted and the lamina is broken down through the action of detergents and reducing agents. Thus, one explanation for the differing results obtained between the immunofluorescence and co-IP experiments is that both the FLAG and GFP tags reduce LaA-Emerin binding (as shown by the co-IP), but that the smaller FLAG tag allows for better integration of LaA into the lamina than the bulky GFP tag, thereby leading to improved nuclear localization of Emerin in cells expressing FLAG-LaA compared to GFP-LaA. In any case, our results suggest that the presence of the bulky N-terminal GFP tag interferes with the ability of LaA to interact with Emerin when LaA is both assembled into the lamina and when the lamina is broken down.

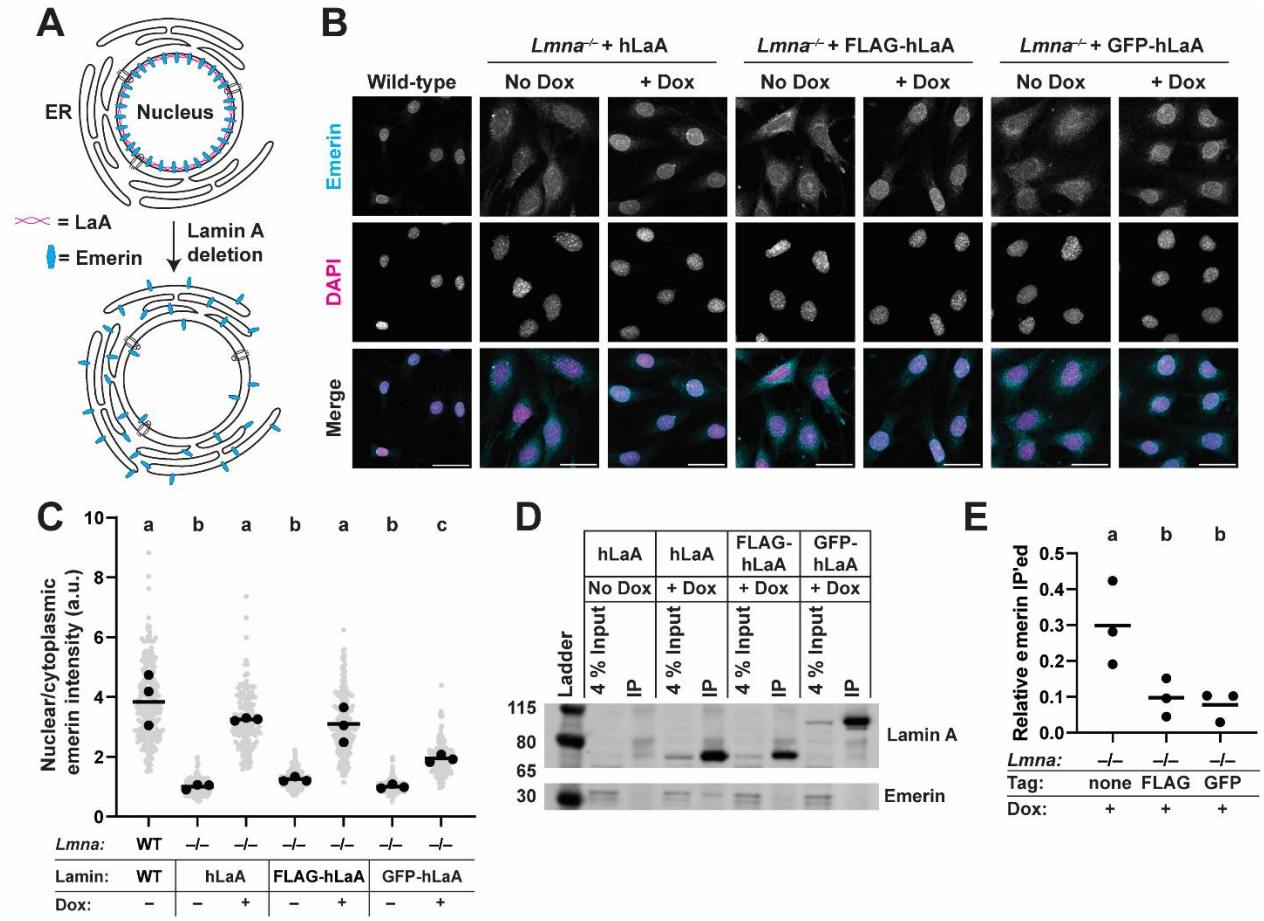

Figure 4: N-terminal tags interfere with the interaction of LaA with Emerin. (**A**) Emerin is mislocalized from the INM to the ER upon loss of lamin A/C. (**B**) Representative immunofluorescence images of wild type and *Lmna*$^{-/-}$

MEFs expressing different LaA constructs and stained for Emerin and DNA (DAPI). Scale bar: 50 µm. (**C**) Quantification of the mean nuclear/cytoplasmic ratios of Emerin immunofluorescence signal in individual cells. Grey points represent measurements from individual cells, black points represent replicate means, and bars indicate overall means. Letters above each set of points indicate results of One-way ANOVA with Tukey's multiple comparison test, performed on the replicate means. Sets of points with the same letter above them are not significantly different, whereas different letters indicate $p < 0.05$. (**D**) Immunoblot of lysates from the indicated cells following immunoprecipitation (IP) with an anti-LaA antibody. 4% of the cell lysate was withheld from the IP experiment and ran on the gel to demonstrate equal amounts of protein in the lysates prior to IP. (**E**) Quantification of Emerin that co-immunoprecipitated with differently tagged lamin constructs. The relative percentage of Emerin immunoprecipitated was quantified by normalizing (dividing) the intensity of the immunoprecipitated Emerin by the input Emerin, and this fraction was normalized to the percentage of LaA that was immunoprecipitated in each experiment.

Taken together, our studies indicate that N-terminal tags perturb some, but not other functions of LaA, with the size of the tag affecting the outcome of only a few functional assays. GFP- and FLAG-tagged LaA were able to perform many of the key functions of the endogenous untagged lamin, and in all assays, we observed at least a partial rescue when the tagged LaA constructs were expressed in *Lmna*$^{-/-}$ MEFs. Furthermore, FLAG- and GFP-tagged LaA were able to completely overcome loss of endogenous lamin A/C in restoring nuclear circularity and nuclear envelope rupture assays. These results are consistent with previous reports *in vivo* using *C. elegans*, where complete loss of lamin is lethal whereas GFP-lamin animals are viable, albeit with fitness defects (Bone et al., 2016). It has also been recently shown that a distantly related lamin homolog in the amoeba *Dictyostelium* can fully complement rates of spontaneous nuclear envelope rupture in *Lmna*$^{-/-}$ MEFs (Odell et al., 2024), consistent with the idea that some functions of LaA can be complemented by a "lamin" that does not completely resemble the wild-type LaA sequence.

In several assays, a clear difference between the tagged versus untagged LaA constructs emerged. In particular, the presence of an N-terminal tag impaired the rescue potential of LaA in terms of proper nuclear envelope localization, nuclear deformability, and interactions with Emerin. We previously showed that in iPSC-derived cardiomyocytes harboring laminopathic LaA mutations, mutant LaA was enriched in the nucleoplasm and led to reduced nuclear stiffness (Wallace et al., 2023), similar to the effects we describe here with FLAG-LaA or GFP-LaA. We propose that both mutant LaA proteins and tagged LaA constructs can alter proper assembly of lamins into higher order filaments. Structural studies have highlighted the importance of the head domain of lamin in the lateral assembly of lamin monomers into dimers, and the ultimate association into higher order filaments (Heitlinger et al., 1992; Zhou et al., 2021). By adding the highly charged FLAG tag or the globular GFP tag to the N-terminus of LaA, these motifs may interrupt the normal assembly dynamics of LaA, leading to an increased pool of unincorporated LaA (Figure 2). This in turn could result in a reduction in the number of filaments or altered filament and lamin network mechanics, leading to the defects observed in the response to the nuclear deformability assay. However, maintenance of nuclear morphology and membrane integrity may not require "perfect" assembly of LaA filaments, which could explain the complete rescue we observed with tagged-LaA constructs in terms of nuclear circularity and rates of nuclear envelope rupture.

The present study has several limitations. One limitation of the co-IP assay is that the antibody used for the co-IP experiments did not recognize endogenous mouse LaA to the same extent as the

exogenous human LaA, and pulldowns using lysates from wild-type MEFs yielded very little LaA, despite the same antibody being able to recognize mouse LaA in fixed cells (see Figure 2A). For this reason, data from wild-type cells are not included in Figure 4D-E. Another limitation of our study is that we express human LaA in mouse fibroblasts, and we cannot fully account for possible species-specific differences between the LaA homologs, although this does not preclude us from making direct comparisons between the different exogenous LaA constructs. We also focus only on LaA and do not consider the effect of tags on lamin C or B-type lamins. Finally, we only tested two specific, commonly used N-terminal tags (i.e., FLAG and GFP) on LaA rescue ability. This leaves open the possibility that other N-terminal tags or internal tags exist that could lead to less severe or no effects on lamin function. Several recent studies reported the use of degron tags fused to lamin (Beer et al., 2019; Pujadas Liwag et al., 2024) or inserted internally within the lamin sequence (Liu et al., 2023), without apparent defects in lamin function; these reports, however, did not present data on the mechanical contributions of tagged lamin to nuclear deformability nor included an expression-controlled comparison to wild-type lamin, as performed in this study, leaving unresolved whether the tag negatively affected some lamin functions.

Overall, our findings may help explain why tagging LaA frequently leads to defects *in vivo* (i.e., in model organisms), even when the tag is present at the endogenous locus and expressed at normal levels. If endogenously tagged lamins have compromised assembly and stiffness, this may result in a decreased ability to resist mechanical stress in vivo, manifesting in decreased viability as observed in *C. elegans* expressing tagged lamin. Furthermore, it is possible that cells expressing tagged LaA may have gene regulatory defects through altered localization of Emerin or other LaA interaction partners, as we observe impaired localization of Emerin and interaction with GFP-tagged LaA. Emerin binds to several important transcriptional regulators and regulates the expression of genes important for skeletal and cardiac muscle function (Koch and Holaska, 2012; Melcon et al., 2006). Thus, it is plausible that altered Emerin dynamics in *C. elegans* expressing tagged lamin could contribute to muscle-specific phenotypes like the swimming defects observed by several groups (Bone et al., 2016; Gregory et al., 2023). Future work using tagged lamins *in vivo* could consider these data and determine if there are transcriptomic changes in organisms that express tagged versions of LaA, which may obscure the interpretations of results obtained with these animals and/or cell lines. Finally, our findings are an important reminder that data obtained with tagged proteins should be interpreted with caution, not only in the context of lamins. Our data indicate that even when some assays suggest normal function of the tagged protein, this does not exclude that other functions are affected by the addition of a tag, even for small tags. Therefore, non-tagged constructs should be included routinely as controls, and if data generated with tagged proteins are central to the conclusion of a study, these findings should be confirmed using non-tagged versions of the protein whenever possible.

Materials and Methods

Cell culture. Spontaneously immortalized wild-type and *Lmna*$^{-/-}$ MEFs were a kind gift from Colin Stewart (Sullivan et al., 1999) and were maintained in DMEM supplemented with 10% FBS and 1% penicillin/streptomycin. Cells were passaged at 80-90% confluency and routinely checked for mycoplasma contamination. For stable genetic manipulations, pseudovirus particles or the Piggybac transposase system were used as described previously (Denais et al., 2016; Earle et al., 2020). Antibiotic selection was performed using Puromycin at 3 µg/ml and Blasticidin at 4.5 µg/ml for at least 1 week. Clonal isolation was performed via serial dilution in a 96-well plate, followed by screening of putative clones by immunofluorescence for homogenous levels of protein expression. Doxycycline titrations were performed in 24-well plates using 1:2 serial dilutions.

Genetic construct information. The doxycycline-inducible FLAG-hLaA construct has been described previously (Odell et al., 2024). Untagged LaA was cloned via Gibson assembly following digestion of the pPB-rtTA-hCas9-puro-PB backbone (Wang et al., 2017) with Nhe1 and Age1. Untagged human LaA was amplified from pCDH-CMV-hLamin_A-IRES-copGFP-EF1-puro (Earle et al., 2020) using the PCR primers 5'-ACCCTCGTAAAGGTCTAGAGACCATGGAGACCCCGTCC-3' and 5'-CCGTTTAAACTCATTACTAATTACATGATGCTGCAGTTCTGG-3'. Enhanced GFP-LaA was cloned into the same backbone following PCR amplification using the PCR primers 5'-ACCCTCGTAAAGGTCTAGAGACCATGGTGAGCAAGGGC-3' and 5'-CCGTTTAAACTCATTACTAATTACATGATGCTGCAGTTCTGG-3'. Following cloning, all constructs were verified with Sanger sequencing of the inserts. The cGAS-mCherry reporter used in this study has been described previously (Denais et al., 2016). For Piggybac transposition, plasmids containing the desired insert were co-transfected with a plasmid encoding a hyperactive transposase (2:1 vector plasmid: hyperactive transposase plasmid) using the Purefection system according to the manufacturer's instructions.

Immunofluorescence. Cells were seeded on fibronectin-coated glass coverslips overnight, then doxycycline was added at the appropriate concentration for 24 h to induce protein expression. Fixation was performed with 4% paraformaldehyde in PBS for 15 minutes at room temperature, followed by 3, 5-minute washes with IF wash buffer containing 2% Triton X, 0.25% Tween 20, and 0.3% BSA in PBS. Cells were blocked in 3% BSA in PBS for 1 hour, then primary antibodies were added for 1h in blocking buffer at room temperature or overnight at 4°C. Primary antibodies used: anti-LaA (Millipore MAB3540, 1:250), Emerin (Leica Emerin-NCL, 1:1000). DAPI was added 1:1000 in PBS for 15 minutes. Secondary antibodies used were Alexa Fluor 488 or 568-conjugated donkey anti mouse/rabbit antibodies (Invitrogen) diluted 1:250 in 3% BSA in PBS. Coverslips were mounted on glass slides using mowiol and kept in the dark until imaging.

Immunoblotting. Cells (1×10^5) were seeded in wells of six-well plates overnight, and then doxycycline was added at the appropriate concentration for 24 h to induce protein expression. Cells were lysed using a high salt RIPA buffer (0.25 g Sodium Deoxycholate; 34.5 ml deionized water [dH2O]; 2.5 ml of 1M Tris pH 8.0; 7.5 ml of 5 M sodium chloride; 5 ml of 10% NP40; 0.5 ml of 10% Sodium dodecyl sulfate). To extract LaA, lysates were vortexed for 5 min, sonicated (Branson 450 Digital Sonifier) for 30 s at 36% amplitude, boiled for 2 min, centrifuged at 4°C for 10 min

and stored at –70°C. Protein concentration was determined using Bradford assay. Equal amounts of protein lysates were denatured in 5 × Laemmli buffer by boiling for 3 min, loaded onto 4–12% Bis-Tris gels (Invitrogen NP0322), run for 1.5 h at 100 V, then transferred for 1 h at 16 V onto PVDF membrane. Membranes were blocked for 1 h in blocking buffer containing 3% BSA in Tris-buffered saline + 1% Tween 20. Primary antibodies used for Figure 1D: rabbit anti Lamin A/C (Cell Signaling 2032S, 1:1000), mouse anti PCNA (Santa Cruz sc-56, 1:1000). Primary antibodies used for Figure 4D: mouse anti LaA (Millipore MAB3540; 1:3000), mouse anti-Emerin (Leica NCL-Emerin; 1:1000). Secondary antibodies used: Licor IRDye 680RD Donkey antiMouse IgG (926-68072) 1:5000, Licor IRDye 800CW Donkey anti-Rabbit IgG (926-32213) 1:5000. Secondary antibodies were added for 1 h at room temperature in blocking buffer, followed by 3 10 min washes. Membranes were imaged using the Odyssey Licor scanner, and then cropped and brightness/ contrast was adjusted using Image Studio Lite (version 5.2) software.

Immunoprecipitation. Co-immunoprecipitation studies were performed using the Pierce Protein A/G magnetic beads (ThermoFisher 88802) according to manufacturer's instructions. Briefly, whole cell lysates were prepared as described above, except the boiling step was omitted to prevent denaturation. Lysates were incubated with anti-LaA antibody (Millipore MAB3540) 1:100 overnight at 4°C with gentle agitation. Magnetic beads (25 µl) were washed 2 times with lysis buffer, then beads were mixed with the lysates and complexes were allowed to form for 1 hour at room temperature with gentle mixing. Bound antibody-antigen complexes were isolated using a magnetic separator, and samples were washed 5 times in IP Wash Buffer containing 50 mM Tris HCl, pH 8.0, 0.3 M NaCl, and 0.3% Triton. Samples were eluted using Laemmli buffer (Biorad 1610737EDU) and boiled for 5 minutes to release bound proteins. The entire volume of eluted protein was loaded onto gels for SDS-PAGE as above, along with 4% lysate input that was set aside prior to addition of primary antibody.

Micropipette aspiration assay. Micropipette aspiration was performed according to a previously published protocol (Davidson et al., 2019). In brief, 1-3 × 10^6 cells were suspended in 2% BSA in PBS supplemented with 0.2% FBS and 10 mM EDTA to prevent cell clumping or adherence. Hoechst was added 1:1000 immediately before the cell suspension was transferred to the micropipette device. Cells were perfused into the device using the following pressure settings: inlet port (top): 1.0 psi; inlet port (bottom): 0.2 psi. Once a flow of cells was established in the device, cells were cleared from the pockets to allow new cells to enter, and images were acquired every 5 s for 40 frames. Nuclear protrusion length was measured using a MatLab script available at (https://github.com/Lammerding/MATLAB-micropipette_analysis).

Microscopy. Confocal images were acquired on a Zeiss LSM900 series confocal microscope with airyscan module using a 40x water immersion objective. The optimal z-slice size was automatically determined using Zen Blue (Zeiss) software. Airy units for images were set between 1.5 and 2.5. Micropipette aspiration data was acquired using an inverted Zeiss Observer Z1 epifluorescence microscope with Hamamatsu Orca Flash 4.0 camera. The image acquisition for micropipette aspiration experiments was automated with Zen Blue (Zeiss) software.

Image analysis. Nuclear circularity calculations were performed using a FIJI macro described in (Odell et al., 2024). Briefly, this macro performs a background subtraction and thresholds the

image based on the DAPI channel to identify nuclei, and then measures the circularity of each nucleus and mean intensity in each channel using the Analyze Particles function.

Intensity profile measurements were performed using a FIJI macro available on request. Briefly, this macro used the "Plot Profile" feature in FIJI to measure the LaA intensity across a line drawn across a z-slice through the center of the nucleus. To account for differences in nuclear size, the intensity profiles are converted into relative nuclear distances, as depicted in Figure 2B.

For measurements of nuclear/cytoplasmic ratios of Emerin, nuclear Emerin was measured using the same macro as the nuclear circularity calculations, and for each cell, cytoplasmic Emerin was obtained by manually drawing a ROI adjacent to the corresponding nucleus for each cell. Then, mean nuclear Emerin intensity was divided by mean cytoplasmic Emerin intensity for each cell.

Nuclear envelope rupture rates were determined based on the fraction of cells positive for nuclear envelope reporter cGAS-mCherry as described previously (Denais et al., 2016; Odell et al., 2024) Briefly, cells were seeded on fibronectin-coated glass coverslips in wells of a 24-well plate, allowed to adhere overnight, and then LaA expression was induced for 24 h using doxycycline concentrations identified in Figure 1. Cells were fixed as above and DNA was labelled using 4',6-diamidino-2-phenylindole (DAPI) diluted 1:1000 in PBS. For counts of cGAS-mCherry positive nuclei, images were blinded and nuclei were scored as "cGAS positive" or "cGAS negative" based on the presence or absence of mCherry puncta adjacent to each DAPI stained nucleus. For all image analysis, cells on the edges of the image, dead cells, or mitotic cells were excluded manually from the analysis.

Statistical analysis and figure generation. All analyses were performed using GraphPad Prism. Information on statistical tests used, cell counts, and significance values are present in each figure caption. Experiments were performed a minimum of three independent times, and for qualitative image analysis, observers were blinded to genotype or treatment conditions when scoring phenotypes. Our statistical analysis was developed in close consultation with the Cornell Statistical Consulting Unit. Figures were assembled using Adobe Illustrator.

Acknowledgements

We thank the Biotechnology Resource Center (BRC) Flow Cytometry Facility (RRID: SCR_021740) and sequencing facility (RRID: SCR_021727) at the Cornell Institute of Biotechnology for their resources and technical assistance. This work was performed in part at the Cornell NanoScale Science & Technology Facility, a member of the National Nanotechnology Coordinated Infrastructure, which is supported by the National Science Foundation (award NNCI-2025233). This work was supported by awards from the Volkswagen Foundation (A130142 to J.L.), the National Institutes of Health (R01 HL082792, R01 GM137605, and R35 GM153257 to J.L.), and the National Science Foundation (URoL2022048 to J.L.). The content of this manuscript is solely the responsibility of the authors and does not necessarily represent the official views of the National Institutes of Health.

References

Aebi, U., Cohn, J., Buhle, L., Gerace, L., 1986. The nuclear lamina is a meshwork of intermediate-type filaments. Nature 323, 560–564. https://doi.org/10.1038/323560a0

Beer, K.B., Fazeli, G., Judasova, K., Irmisch, L., Causemann, J., Mansfeld, J., Wehman, A.M., 2019. Degron-tagged reporters probe membrane topology and enable the specific labelling of membrane-wrapped structures. Nat Commun 10, 3490. https://doi.org/10.1038/s41467-019-11442-z

Bone, C.R., Chang, Y.-T., Cain, N.E., Murphy, S.P., Starr, D.A., 2016. Nuclei migrate through constricted spaces using microtubule motors and actin networks in C. elegans hypodermal cells. Development 143, 4193–4202. https://doi.org/10.1242/dev.141192

Borin, D., Peña, B., Taylor, M.R.G., Mestroni, L., Lapasin, R., Sbaizero, O., 2020. Viscoelastic behavior of cardiomyocytes carrying LMNA mutations. Biorheology 57, 1–14. https://doi.org/10.3233/BIR-190229

Broers, J.L.V., Machiels, B.M., van Eys, G.J.J.M., Kuijpers, H.J.H., Manders, E.M.M., van Driel, R., Ramaekers, F.C.S., 1999. Dynamics of the nuclear lamina as monitored by GFP-tagged A-type lamins. Journal of Cell Science 112, 3463–3475. https://doi.org/10.1242/jcs.112.20.3463

Buxboim, A., Kronenberg-Tenga, R., Salajkova, S., Avidan, N., Shahak, H., Thurston, A., Medalia, O., 2023. Scaffold, mechanics and functions of nuclear lamins. FEBS Letters 597, 2791–2805. https://doi.org/10.1002/1873-3468.14750

Chen, N.Y., Kim, P., Weston, T.A., Edillo, L., Tu, Y., Fong, L.G., Young, S.G., 2018. Fibroblasts lacking nuclear lamins do not have nuclear blebs or protrusions but nevertheless have frequent nuclear membrane ruptures. Proc Natl Acad Sci U S A 115, 10100–10105. https://doi.org/10.1073/pnas.1812622115

Chen, N.Y., Kim, P.H., Tu, Y., Yang, Y., Heizer, P.J., Young, S.G., Fong, L.G., 2021. Increased expression of LAP2β eliminates nuclear membrane ruptures in nuclear lamin-deficient neurons and fibroblasts. Proc Natl Acad Sci U S A 118, e2107770118. https://doi.org/10.1073/pnas.2107770118

Cho, S., Vashisth, M., Abbas, A., Majkut, S., Vogel, K., Xia, Y., Ivanovska, I.L., Irianto, J., Tewari, M., Zhu, K., Tichy, E.D., Mourkioti, F., Tang, H.-Y., Greenberg, R.A., Prosser, B.L., Discher, D.E., 2019. Mechanosensing by the Lamina Protects against Nuclear Rupture, DNA Damage, and Cell-Cycle Arrest. Dev Cell 49, 920-935.e5. https://doi.org/10.1016/j.devcel.2019.04.020

Coffinier, C., Jung, H.-J., Li, Z., Nobumori, C., Yun, U.J., Farber, E.A., Davies, B.S., Weinstein, M.M., Yang, S.H., Lammerding, J., Farahani, J.N., Bentolila, L.A., Fong, L.G., Young, S.G., 2010. Direct synthesis of lamin A, bypassing prelamin a processing, causes misshapen nuclei in fibroblasts but no detectable pathology in mice. J Biol Chem 285, 20818–20826. https://doi.org/10.1074/jbc.M110.128835

Davidson, P.M., R. Fedorchak, G., Mondésert-Deveraux, S., S. Bell, E., Isermann, P., Aubry, D., Allena, R., Lammerding, J., 2019. High-throughput microfluidic micropipette aspiration device to probe time-scale dependent nuclear mechanics in intact cells. Lab on a Chip 19, 3652–3663. https://doi.org/10.1039/C9LC00444K

de Leeuw, R., Gruenbaum, Y., Medalia, O., 2018. Nuclear Lamins: Thin Filaments with Major Functions. Trends Cell Biol 28, 34–45. https://doi.org/10.1016/j.tcb.2017.08.004

De Vos, W.H., Houben, F., Kamps, M., Malhas, A., Verheyen, F., Cox, J., Manders, E.M.M., Verstraeten, V.L.R.M., van Steensel, M.A.M., Marcelis, C.L.M., van den Wijngaard, A.,

Vaux, D.J., Ramaekers, F.C.S., Broers, J.L.V., 2011. Repetitive disruptions of the nuclear envelope invoke temporary loss of cellular compartmentalization in laminopathies. Hum Mol Genet 20, 4175–4186. https://doi.org/10.1093/hmg/ddr344

Denais, C.M., Gilbert, R.M., Isermann, P., McGregor, A.L., te Lindert, M., Weigelin, B., Davidson, P.M., Friedl, P., Wolf, K., Lammerding, J., 2016. Nuclear envelope rupture and repair during cancer cell migration. Science 352, 353–358. https://doi.org/10.1126/science.aad7297

Dou, Z., Xu, C., Donahue, G., Shimi, T., Pan, J.-A., Zhu, J., Ivanov, A., Capell, B.C., Drake, A.M., Shah, P.P., Catanzaro, J.M., Daniel Ricketts, M., Lamark, T., Adam, S.A., Marmorstein, R., Zong, W.-X., Johansen, T., Goldman, R.D., Adams, P.D., Berger, S.L., 2015. Autophagy mediates degradation of nuclear lamina. Nature 527, 105–109. https://doi.org/10.1038/nature15548

Earle, A.J., Kirby, T.J., Fedorchak, G.R., Isermann, P., Patel, J., Iruvanti, S., Moore, S.A., Bonne, G., Wallrath, L.L., Lammerding, J., 2020. Mutant lamins cause nuclear envelope rupture and DNA damage in skeletal muscle cells. Nat Mater 19, 464–473. https://doi.org/10.1038/s41563-019-0563-5

Fernandez, A., Bautista, M., Wu, L., Pinaud, F., 2022. Emerin self-assembly and nucleoskeletal coupling regulate nuclear envelope mechanics against stress. J Cell Sci 135, jcs258969. https://doi.org/10.1242/jcs.258969

Gregory, E.F., Ragle, J.M., Ward, J.D., Starr, D.A., 2023. Split-GFP lamin as a tool for studying C. elegans LMN-1 dynamics in vivo. microPublication Biology. https://doi.org/10.17912/micropub.biology.001022

Guo, Y., Kim, Y., Shimi, T., Goldman, R.D., Zheng, Y., 2014. Concentration-dependent lamin assembly and its roles in the localization of other nuclear proteins. MBoC 25, 1287–1297. https://doi.org/10.1091/mbc.e13-11-0644

Gurudatta, B.V., Shashidhara, L.S., Parnaik, V.K., 2010. Lamin C and chromatin organization in Drosophila. J Genet 89, 37–49. https://doi.org/10.1007/s12041-010-0009-y

Heitlinger, E., Peter, M., Lustig, A., Villiger, W., Nigg, E.A., Aebi, U., 1992. The role of the head and tail domain in lamin structure and assembly: Analysis of bacterially expressed chicken Lamin A and truncated B2 lamins. Journal of Structural Biology 108, 74–91. https://doi.org/10.1016/1047-8477(92)90009-Y

Herrmann, H., Hesse, M., Reichenzeller, M., Aebi, U., Magin, T.M., 2002. Functional complexity of intermediate filament cytoskeletons: From structure to assembly to gene ablation, in: International Review of Cytology. Academic Press, pp. 83–175. https://doi.org/10.1016/S0074-7696(05)23003-6

Kalukula, Y., Stephens, A.D., Lammerding, J., Gabriele, S., 2022. Mechanics and functional consequences of nuclear deformations. Nat Rev Mol Cell Biol 23, 583–602. https://doi.org/10.1038/s41580-022-00480-z

Koch, A.J., Holaska, J.M., 2012. Loss of emerin alters myogenic signaling and miRNA expression in mouse myogenic progenitors. PLoS One 7, e37262. https://doi.org/10.1371/journal.pone.0037262

Kono, Y., Adam, S.A., Sato, Y., Reddy, K.L., Zheng, Y., Medalia, O., Goldman, R.D., Kimura, H., Shimi, T., 2022. Nucleoplasmic lamin C rapidly accumulates at sites of nuclear envelope rupture with BAF and cGAS. Journal of Cell Biology 221, e202201024. https://doi.org/10.1083/jcb.202201024

Kreplak, L., Richter, K., Aebi, U., Herrmann, H., 2008. Chapter 15 Electron Microscopy of Intermediate Filaments: Teaming up with Atomic Force and Confocal Laser Scanning Microscopy, in: Methods in Cell Biology, Introduction to Electron Microscopy for Biologists. Academic Press, pp. 273–297. https://doi.org/10.1016/S0091-679X(08)00415-9

Lammerding, J., Fong, L.G., Ji, J.Y., Reue, K., Stewart, C.L., Young, S.G., Lee, R.T., 2006. Lamins A and C but Not Lamin B1 Regulate Nuclear Mechanics*. Journal of Biological Chemistry 281, 25768–25780. https://doi.org/10.1074/jbc.M513511200

Lammerding, J., Schulze, P.C., Takahashi, T., Kozlov, S., Sullivan, T., Kamm, R.D., Stewart, C.L., Lee, R.T., 2004. Lamin A/C deficiency causes defective nuclear mechanics and mechanotransduction. J Clin Invest 113, 370–378. https://doi.org/10.1172/JCI19670

Liddane, A.G., Holaska, J.M., 2021. The Role of Emerin in Cancer Progression and Metastasis. Int J Mol Sci 22, 11289. https://doi.org/10.3390/ijms222011289

Liu, C., Rex, R., Lung, Z., Wang, J.S., Wu, F., Kim, H.J., Zhang, L., Sohn, L.L., Dernburg, A.F., 2023. A cooperative network at the nuclear envelope counteracts LINC-mediated forces during oogenesis in C. elegans. Science Advances 9, eabn5709. https://doi.org/10.1126/sciadv.abn5709

Manju, K., Muralikrishna, B., Parnaik, V.K., 2006. Expression of disease-causing lamin A mutants impairs the formation of DNA repair foci. Journal of Cell Science 119, 2704–2714. https://doi.org/10.1242/jcs.03009

Melcon, G., Kozlov, S., Cutler, D.A., Sullivan, T., Hernandez, L., Zhao, P., Mitchell, S., Nader, G., Bakay, M., Rottman, J.N., Hoffman, E.P., Stewart, C.L., 2006. Loss of emerin at the nuclear envelope disrupts the Rb1/E2F and MyoD pathways during muscle regeneration. Hum Mol Genet 15, 637–651. https://doi.org/10.1093/hmg/ddi479

Morin, X., Daneman, R., Zavortink, M., Chia, W., 2001. A protein trap strategy to detect GFP-tagged proteins expressed from their endogenous loci in Drosophila. Proceedings of the National Academy of Sciences 98, 15050–15055. https://doi.org/10.1073/pnas.261408198

Odell, J., Gräf, R., Lammerding, J., 2024. Heterologous expression of Dictyostelium discoideum NE81 in mouse embryo fibroblasts reveals conserved mechanoprotective roles of lamins. MBoC 35, ar7. https://doi.org/10.1091/mbc.E23-05-0193

Odell, J., Lammerding, J., 2023. Lamins as structural nuclear elements through evolution. Current Opinion in Cell Biology 85, 102267. https://doi.org/10.1016/j.ceb.2023.102267

Östlund, C., Sullivan, T., Stewart, C.L., Worman, H.J., 2006. Dependence of Diffusional Mobility of Integral Inner Nuclear Membrane Proteins on A-Type Lamins. Biochemistry 45, 1374–1382. https://doi.org/10.1021/bi052156n

Pajerowski, J.D., Dahl, K.N., Zhong, F.L., Sammak, P.J., Discher, D.E., 2007. Physical plasticity of the nucleus in stem cell differentiation. Proceedings of the National Academy of Sciences 104, 15619–15624. https://doi.org/10.1073/pnas.0702576104

Pujadas Liwag, E.M., Wei, X., Acosta, N., Carter, L.M., Yang, J., Almassalha, L.M., Jain, S., Daneshkhah, A., Rao, S.S.P., Seker-Polat, F., MacQuarrie, K.L., Ibarra, J., Agrawal, V., Aiden, E.L., Kanemaki, M.T., Backman, V., Adli, M., 2024. Depletion of lamins B1 and B2 promotes chromatin mobility and induces differential gene expression by a mesoscale-motion-dependent mechanism. Genome Biol 25, 77. https://doi.org/10.1186/s13059-024-03212-y

Raab, M., Gentili, M., de Belly, H., Thiam, H.R., Vargas, P., Jimenez, A.J., Lautenschlaeger, F., Voituriez, R., Lennon-Duménil, A.M., Manel, N., Piel, M., 2016. ESCRT III repairs nuclear envelope ruptures during cell migration to limit DNA damage and cell death. Science 352, 359–362. https://doi.org/10.1126/science.aad7611

Rizzo, M.A., Davidson, M.W., Piston, D.W., 2009. Fluorescent Protein Tracking and Detection: Applications Using Fluorescent Proteins in Living Cells. Cold Spring Harb Protoc 2009, pdb.top64. https://doi.org/10.1101/pdb.top64

Roux, K.J., Kim, D.I., Raida, M., Burke, B., 2012. A promiscuous biotin ligase fusion protein identifies proximal and interacting proteins in mammalian cells. Journal of Cell Biology 196, 801–810. https://doi.org/10.1083/jcb.201112098

Schulze, S.R., Curio-Penny, B., Li, Y., Imani, R.A., Rydberg, L., Geyer, P.K., Wallrath, L.L., 2005. Molecular genetic analysis of the nested Drosophila melanogaster lamin C gene. Genetics 171, 185–196. https://doi.org/10.1534/genetics.105.043208

Shimi, T., Kittisopikul, M., Tran, J., Goldman, A.E., Adam, S.A., Zheng, Y., Jaqaman, K., Goldman, R.D., 2015. Structural organization of nuclear lamins A, C, B1, and B2 revealed by superresolution microscopy. Mol Biol Cell 26, 4075–4086. https://doi.org/10.1091/mbc.E15-07-0461

Sinensky, M., Fantle, K., Trujillo, M., McLain, T., Kupfer, A., Dalton, M., 1994. The processing pathway of prelamin A. J Cell Sci 107 (Pt 1), 61–67. https://doi.org/10.1242/jcs.107.1.61

Srivastava, L.K., Ju, Z., Ghagre, A., Ehrlicher, A.J., 2021. Spatial distribution of lamin A/C determines nuclear stiffness and stress-mediated deformation. J Cell Sci 134, jcs248559. https://doi.org/10.1242/jcs.248559

Stephens, A.D., Banigan, E.J., Adam, S.A., Goldman, R.D., Marko, J.F., 2017. Chromatin and lamin A determine two different mechanical response regimes of the cell nucleus. Mol Biol Cell 28, 1984–1996. https://doi.org/10.1091/mbc.E16-09-0653

Sullivan, T., Escalante-Alcalde, D., Bhatt, H., Anver, M., Bhat, N., Nagashima, K., Stewart, C.L., Burke, B., 1999. Loss of a-Type Lamin Expression Compromises Nuclear Envelope Integrity Leading to Muscular Dystrophy. Journal of Cell Biology 147, 913–920. https://doi.org/10.1083/jcb.147.5.913

Swift, J., Ivanovska, I.L., Buxboim, A., Harada, T., Dingal, P.C.D.P., Pinter, J., Pajerowski, J.D., Spinler, K.R., Shin, J.-W., Tewari, M., Rehfeldt, F., Speicher, D.W., Discher, D.E., 2013. Nuclear Lamin-A Scales with Tissue Stiffness and Enhances Matrix-Directed Differentiation. Science 341, 1240104. https://doi.org/10.1126/science.1240104

Vahabikashi, A., Adam, S.A., Medalia, O., Goldman, R.D., 2022. Nuclear lamins: Structure and function in mechanobiology. APL Bioengineering 6, 011503. https://doi.org/10.1063/5.0082656

Vaughan, O.A., Alvarez-Reyes, M., Bridger, J.M., Broers, J.L.V., Ramaekers, F.C.S., Wehnert, M., Morris, G.E., Whitfield, W.G.F., Hutchison, C.J., 2001. Both emerin and lamin C depend on lamin A for localization at the nuclear envelope. Journal of Cell Science 114, 2577–2590. https://doi.org/10.1242/jcs.114.14.2577

Velez-Aguilera, G., Nkombo Nkoula, S., Ossareh-Nazari, B., Link, J., Paouneskou, D., Van Hove, L., Joly, N., Tavernier, N., Verbavatz, J.-M., Jantsch, V., Pintard, L., 2020. PLK-1 promotes the merger of the parental genome into a single nucleus by triggering lamina disassembly. eLife 9, e59510. https://doi.org/10.7554/eLife.59510

Wallace, M., Zahr, H., Perati, S., Morsink, C.D., Johnson, L.E., Gacita, A.M., Lai, S., Wallrath, L.L., Benjamin, I.J., McNally, E.M., Kirby, T.J., Lammerding, J., 2023. Nuclear damage

in LMNA mutant iPSC-derived cardiomyocytes is associated with impaired lamin localization to the nuclear envelope. MBoC 34, ar113. https://doi.org/10.1091/mbc.E21-10-0527

Wang, G., Yang, L., Grishin, D., Rios, X., Ye, L.Y., Hu, Y., Li, K., Zhang, D., Church, G.M., Pu, W.T., 2017. Efficient, footprint-free human iPSC genome editing by consolidation of Cas9/CRISPR and piggyBac technologies. Nat Protoc 12, 88–103. https://doi.org/10.1038/nprot.2016.152

Wintner, O., Hirsch-Attas, N., Schlossberg, M., Brofman, F., Friedman, R., Kupervaser, M., Kitsberg, D., Buxboim, A., 2020. A Unified Linear Viscoelastic Model of the Cell Nucleus Defines the Mechanical Contributions of Lamins and Chromatin. Adv Sci (Weinh) 7, 1901222. https://doi.org/10.1002/advs.201901222

Zhou, X., Lin, Y., Kato, M., Mori, E., Liszczak, G., Sutherland, L., Sysoev, V.O., Murray, D.T., Tycko, R., McKnight, S.L., 2021. Transiently structured head domains control intermediate filament assembly. Proceedings of the National Academy of Sciences 118, e2022121118. https://doi.org/10.1073/pnas.2022121118

Zwerger, M., Jaalouk, D.E., Lombardi, M.L., Isermann, P., Mauermann, M., Dialynas, G., Herrmann, H., Wallrath, L.L., Lammerding, J., 2013. Myopathic lamin mutations impair nuclear stability in cells and tissue and disrupt nucleo-cytoskeletal coupling. Hum Mol Genet 22, 2335–2349. https://doi.org/10.1093/hmg/ddt079

Zwerger, M., Roschitzki-Voser, H., Zbinden, R., Denais, C., Herrmann, H., Lammerding, J., Grütter, M.G., Medalia, O., 2015. Altering lamina assembly reveals lamina-dependent and -independent functions for A-type lamins. J Cell Sci 128, 3607–3620. https://doi.org/10.1242/jcs.171843